LANGMUIR

pubs.acs.org/Langmuir Article

Determining the Characteristics of Ultrathin Polymer Films: A Spectroscopic Ellipsometry Approach

Sonam Zangpo Bhutia, Sathish K. Sukumaran,* and Dillip K. Satapathy*

Cite This: *Langmuir* 2024, 40, 14153−14165 Read Online

ACCESS | Metrics & More | Article Recommendations | Supporting Information

ABSTRACT: Ellipsometry is a powerful and convenient technique that is widely used to determine the thickness and optical characteristics of polymer thin films. The determination is accomplished by modeling the measured change in the polarization of an electromagnetic wave upon interacting with the thin film. However, due to the strong statistical correlations between the fit parameters in the model, simultaneous determination of the thickness and the refractive indices of optically anisotropic ultrathin films using ellipsometry remains a challenge. Here, we propose an approach that can be used to obtain reliable values of both the thickness and the optical anisotropy of ultrathin polymer films. The approach was developed by performing spectroscopic ellipsometry measurements on thin films of hydrophobic polystyrene and hydrophilic chitosan of thickness between a few tens to a few hundred nm and whose absolute value of the birefringence differed by approximately an order of magnitude. Careful consideration of the characteristics of the root mean squared error of the fits obtained by modeling the ellipsometry data and the statistical correlations between the fit parameters formed the basis of the proposed approach.

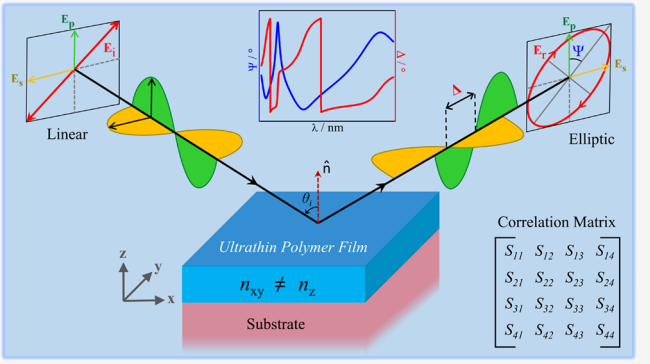

INTRODUCTION

Understanding and predicting the physical properties of polymer thin films, whether substrate-supported or free-standing, are crucial not only from a fundamental point of view but also for the development of functional nanoscale devices.[1] Polymer thin films deposited on hard substrates are particularly significant due to the plethora of choices for both the polymer and the substrate, as well as the ease with which the film thickness can be varied. Given that polymer chains cannot penetrate into the hard substrate, polymer chains in a thin film are subject to one-dimensional confinement. At least partly due to this one-dimensional confinement, conformations and dynamics of the polymer chains, and consequently, various properties of polymer thin films, are strongly affected by the thin film thickness. Confinement of polymer chains at the nanoscale, say in a thin film, has been demonstrated to significantly influence the dynamics of the chains.[2,3] This results in observable effects on various physical properties, including but not limited to the melting temperature and the glass transition temperature of the thin film.[4] Therefore, techniques for accurately determining the thickness of polymer thin films are of paramount importance.

Ellipsometry has emerged as a technique of choice as it can nondestructively determine the thickness of thin films with sufficient accuracy. In addition, the technique is highly versatile considering the wide range of materials (metals, polymers etc.), phases (solids and liquids), and environmental conditions (temperature, humidity etc.) under which thin films can be investigated. Recent developments in hardware and software have rendered the technique particularly easy to use[5−10] not only on single-layer but also on multilayer thin films.[11,12] The aforementioned features, when combined, have enabled the widespread use of the technique in a range of industries from semiconductors[13] to medicine.[14] For instance, ellipsometry has been extensively used to investigate thermal transitions,[15,16] especially the glass transition,[17−19] swelling kinetics in the presence of various solvents and their vapors,[20−25] and optical anisotropy[20,24,26−34] in a wide range of polymeric systems, including homopolymers, copolymers, and composites.

Polymer thin films can exhibit optical anisotropy depending on the film thickness, preparation conditions, polymer−substrate interactions, polymer molecular weight etc.[35−37] The optical anisotropy can be conveniently expressed using the negative of the birefringence, Δn (defined later),[24,29,35−37] and can be positive or negative. For instance, using micrometer

Received: May 11, 2024
Revised: June 12, 2024
Accepted: June 13, 2024
Published: June 24, 2024

https://doi.org/10.1021/acs.langmuir.4c01761
Langmuir 2024, 40, 14153−14165

thick films of PS, it has been determined that $\Delta n \approx -0.0061$ at the incident wavelength, $\lambda \approx 633$ nm.[36] In contrast and consistent with the measurements of Nosal et al.,[31] for chitosan $\Delta n \approx 0.016$ at $\lambda \approx 633$ nm.[24] For polymer thin films, ellipsometry offers a rapid, reliable, and robust route for the determination of birefringence.[24,26−31,34,38]

The sensitivity of ellipsometry data to the values of the fit parameters varies with the particular angles of incidence (AOI) and the range of wavelengths, λ, used for the measurement. For instance, AOI close to the Brewster's angle, θ_B, are considered near optimal where the ellipsometry measurement is expected to exhibit high sensitivity[39−41] to the values of the fit parameters. Given that for silicon (Si), $\theta_B \approx 74°$ at $\lambda \approx 633$ nm,[40−42] and partly for historical reasons,[40] ellipsometric measurements of polymer thin films on Si substrates are commonly performed at an AOI $\approx 70°$.[15,24,25,40,41,43,44] Similarly, for glass substrates, as the $\theta_B \approx 55°$ at $\lambda \approx 633$ nm,[41,45] measurements are performed at an AOI $\approx 60°$.[46,47] In summary, most measurements on thin films are performed at an AOI between 45° and 80°.[18,24,25,28−30,38,40−43,48,49] Therefore, depending on the range of variation of the physical quantities under investigation, this necessitated preparatory experiments to identify the optimal AOI and λ at which the data were most sensitively dependent on the values of the parameters to be determined from the fits.[17,29,39−41,48] However, such preparatory experiments become unnecessary when using Variable Angle Spectroscopic Ellipsometry (VASE) capable of measuring at multiple AOI and λ.

Ellipsometry is conventionally used for determining the thickness, d, and the optical properties of thin films, such as their refractive indices. For thin films with $d \geq 30$ nm, past literature suggests that the refractive indices can be determined with sufficient accuracy.[33,41,48] For instance, Guo et al.[48] concluded that combining ellipsometry with another technique that can measure the film thickness, such as profilometry, enables the accurate determination of the isotropic refractive index, n_{iso}, and the thickness of relatively thick transparent polymer films. By quantifying the rate of change of n_{iso} with the film thickness, d, they argued that the accuracy of the determination of n_{iso} decreased with decreasing d.[48] In line with this, accurate determination of the refractive indices for $d \leq 30$ nm[41] has remained a serious challenge as ellipsometry is unable to simultaneously and uniquely determine the d and the refractive indices.[18,21,33,48,50,51] The aforementioned non-uniqueness stems from the strong statistical correlations that exist between the d and the refractive indices in such ultrathin films.[18,33,48,52]

In this study, we have focused on thin films of PS and chitosan as the absolute values of their birefringence vary by approximately an order of magnitude. For these two polymers, we present systematic investigations of the optical properties for $12 \leq d \leq 312$ nm. In particular, we have explored the dependence of root mean squared error (RMSE) on the d and the refractive indices, as well as the statistical correlations between the various fit parameters. On the basis of these findings, we propose an approach to data fitting whereby the d and the anisotropic refractive indices, and consequently the birefringence, can be reliably determined for thin films even when $d \leq 30$ nm using only VASE.

EXPERIMENTAL SECTION

Materials and Methods. The PS and chitosan were obtained in powder form from Sigma-Aldrich and used as received. The molecular weight of PS was in the range of 360,000−460,000 g/mol resulting in $2R_g \approx 32−36$ nm. The degree of deacetylation of chitosan, as indicated by the manufacturer, was 75−85%, and the molecular weight was in the range of 50,000−190,000 g/mol, resulting in $2R_g \approx 37−73$ nm. Thin films of each polymer were fabricated using a Polos spin150i spin coater (SPS-Europe). The films were prepared as follows.

Preparation of PS Thin Films. PS solutions of concentrations ranging from 0.1 to 3.5 wt % were prepared by dissolving PS in toluene and stirring magnetically for 2 h at 50 °C. The solution was cooled to room temperature and filtered through 0.22 μm nylon syringe filters. Si wafers were cleaved into 1 cm × 1 cm pieces and treated in piranha solution ($3H_2SO_4$:H_2O_2) at 80 °C for at least 30 min to eliminate organic contaminants. The Si wafer substrates were rinsed thoroughly with deionized water (resistivity = 18.2 MΩ cm) and dipped in hydrofluoric acid solution (5 vol %) for 5 min to achieve a hydrophobic Si/Si−H surface. Despite the hydrofluoric acid treatment and likely due to exposure to ambient oxygen, a 1.15 nm SiO_2 layer was found to exist on the substrate surface. Past literature has reported the presence of an oxide layer of thickness of approximately 1.3 nm after a similar treatment with an aqueous hydrofluoric acid solution.[49,53] After rinsing the substrates with deionized water and flushing with dry nitrogen gas, the substrate was placed inside the spin coater and accelerated to 3000 at 100 rpm/s. PS solutions of different concentrations were spin-coated at the top speed for 60 s to prepare thin films of varying thicknesses.

Preparation of Chitosan Thin Films. Chitosan solutions of concentrations ranging from 0.5 to 2.75 wt % were prepared by dissolving the polymer in a (5% acetic acid)/water solution and stirring magnetically for 5 h at 50 °C. After cooling to room temperature, the solutions were filtered through 1.6 μm syringe filters. Si wafers were cleaved into 1 cm × 1 cm pieces and treated with piranha solution ($3H_2SO_4$:H_2O_2) at 80 °C for at least 30 min to eliminate organic contaminants and render the surface hydrophilic. After thoroughly rinsing with DI water and flushing with dry nitrogen gas, the substrates retained a SiO_2 layer of thickness of approximately 2 nm. Past literature has reported the presence of an oxide layer of similar thickness after such a treatment.[24,25,34,54] Thin films of chitosan of varying thicknesses were produced by spin coating for 60 s at maximum speeds ranging from 3000 to 9000 rpm achieved using rotational accelerations of either 60 or 100 rpm/s.

The aforementioned processes ensured the consistent fabrication of PS[18,49,53] and chitosan[24,55] thin films of desired thicknesses. To remove any residual solvent, the freshly prepared PS and chitosan thin films were dried for 12 h in a vacuum oven maintained at 130 °C. Following this, the films were allowed to cool to room temperature and were stored in a vacuum desiccator until further characterization.

Spectroscopic Ellipsometry (SE). SE is a contact-less non-destructive optical technique based on the measurement of the change in the polarization state of incident light upon reflection or transmission. The technique has proven to be a powerful tool for measuring several crucial optical properties, such as the film thickness, refractive indices, or dielectric constants of thin films of various types with high precision and accuracy.[18,39−41,52,54,56−58]

The changes in the polarization state are conventionally described by the ellipsometric angles Ψ and Δ. The Ψ is defined using $\tan(\Psi) \equiv |r_p|/|r_s|$, where the subscript p indicates the electric field component of the incident light in the plane of incidence (parallel) and s indicates the component perpendicular to it. The Δ is defined using $\Delta \equiv \delta_i - \delta_r$, where δ_i and δ_r are the phase differences between the p and s components before and after reflection, respectively. The fundamental equation of ellipsometry can be written as[40,44,48,54,57]

$$\rho = \frac{r_p}{r_s} = \tan(\Psi)e^{i\Delta} = f(\lambda, \theta_0, d_i, \tilde{N}_0, \tilde{N}_i, \tilde{N}_s) \quad (1)$$

where the Ψ and Δ are related to the complex reflectance function, ρ, given by the ratio of the total reflection coefficients r_p and r_s. Therefore, it can be seen that Ψ and Δ are functions of several parameters such as the source wavelength, λ; the incidence angle, θ_0;

https://doi.org/10.1021/acs.langmuir.4c01761
Langmuir 2024, 40, 14153−14165

the thickness of each layer atop the substrate, d_i; and the complex refractive indices ($\tilde{N} \equiv n - ik$) of the ambient medium $\tilde{N}_0$, of each individual layer $\tilde{N}_i$, and the substrate $\tilde{N}_s$. Instead of directly measuring Ψ and Δ, several modern ellipsometers utilize three of the Stokes parameters to describe the polarization state of the light. For additional details, refer section "Root Mean Squared Error (RMSE)" of the Supporting Information.

For the SE measurements, we employed a variable angle multiwavelength (370−1688 nm) ellipsometer (J.A. Woollam Co., USA) equipped with CompleteEASE software for data analysis. The software utilizes the Levenberg−Marquardt algorithm to perform iterative nonlinear regression fits,[9,31,39,58,59] in order to minimize the RMSE by adjusting the values of the fit parameters. The fits result in optimal values for thickness, surface and/or interfacial roughness, and optical constants. To achieve the best fits, two conditions should be satisfied: (i) the constructed optical model must accurately describe the sample and (ii) the initial values of fit parameters should be reasonably close to their physical values. The CompleteEASE software addresses these requirements effectively. First, the "Try Alternate Models" feature enables the selection of the most suitable model by trying several model fits. Second, the "Thickness Pre-Fit" and the "Global Fit" options perform numerous trial fits by varying the initial values of the fitting parameters. SE measurements were conducted using an illumination spot with a diameter of 2 mm on the sample, covering multiple AOI from 50° to 75° in 5° increments. The data acquisition time for each measurement at a specific angle was 5 s. To account for the depolarization of reflected light due to intensity loss and phase change,[34,52,57] the depolarization parameter was included in all of the fits.

Optical Model for Data Interpretation. The measured λ dependence of Ψ and Δ was modeled using the CompleteEASE software. As the thin film samples were verified to be optically transparent (extinction coefficient, $k \approx 0$), the λ dependence of the refractive index can be modeled using the Cauchy dispersion equation given by,

$$n(\lambda) = A + \frac{B}{\lambda^2} + \frac{C}{\lambda^4} \tag{2}$$

where the A, B, and C are fit parameters. The C in eq 2 has often been set to 0 without significantly affecting the quality of the fits.[23−25,33,41,46] In the current work, we have verified that the inclusion of the term corresponding to C reduced the RMSE by less than 0.5%. In addition, the values of B and C were highly correlated which suggested that one of the two might be redundant. Therefore, in all our fits to eq 2, we have set C to 0.

The optical characteristics of materials can typically be classified into either isotropic or anisotropic. A material with identical optical properties (such as the index of refraction, n) along different light propagation directions x, y, and z is termed optically isotropic, i.e., $n_x = n_y = n_z$. In contrast, a material with distinct optical properties along different light propagation directions is termed optically anisotropic. Optically anisotropic materials where $n_x \neq n_y \neq n_z$ are termed biaxially anisotropic. Polymer thin films, however, are uniaxially anisotropic,[24,26,29−32,34] where the index of refraction within the plane satisfies $n_x = n_y \equiv n_{xy}$. The in-plane index of refraction, n_{xy}, differs from the out-of-plane index of refraction, n_z, i.e., $n_{xy} \neq n_z$, with the optic axis being along the z direction. A measure of the optical anisotropy can be defined using the negative of the birefringence, $\Delta n \equiv n_{xy} - n_z$. Remarkably, SE is sensitive enough to measure changes in n of 0.001.[24,31,33] Hence, Δn of similar magnitude can be reliably measured. The Cauchy equation introduced above, eq 2, can be used to describe the λ dependence of the refractive index for both isotropic and anisotropic materials. In anisotropic materials, each refractive index of interest needs to be described by a separate Cauchy equation. For instance, in uniaxially anisotropic materials, both the n_{xy} and the n_z can be described by Cauchy equations but with different values of the fitting parameters.

Goodness of Fit. Quantitative characterization of how well the model can describe the experimental data can be accomplished using the RMSE and/or the correlation matrix.[33,41,52,58]

Root Mean Squared Error (RMSE). The RMSE is arguably the most widely used parameter to consider the quality of a fit as it directly quantifies the deviation or error between the experimentally measured and the model-generated curves for Ψ and Δ.[9,40,52,58] Further details are provided in the section "Root Mean Squared Error (RMSE)" of the Supporting Information. Lower values of RMSE indicate better fits. It is recommended that only the minimum number of parameters necessary to adequately describe the experimental data be used. As a general guideline, increasing the number of fit parameters by one is considered justified only when it leads to a reduction in RMSE of at least 20−25%.[33,40,41,58]

Correlation Matrix. Another quantity of interest is the correlation matrix whose elements are the correlation coefficients, S_{ij}, between any two fit parameters i and j. The correlation coefficient S_{ij} can be defined as

$$S_{ij} = \frac{c_{ij}}{\sqrt{c_{ii}}\sqrt{c_{jj}}} \tag{3}$$

where c_{ij} is the element of the covariance matrix of the fitting parameters.[24,28,30] The absolute value of the correlation coefficient, $|S_{ij}|$, between any two parameters approaching 1 is a strong indication that one of the two parameters is redundant. Such highly correlated parameters indicate that the used model has been overparameterized and the values of the fit parameters obtained using such a model are not unique.[28,30,58]

X-Ray Reflectivity (XRR). To obtain independent measurements of the film thickness, we employed X-ray reflectivity (XRR).[60−62] The thin film samples were illuminated using parallel Cu−Kα radiation ($\lambda_{Cu-K\alpha}$ = 1.5406 Å) to perform a 2θ scan from 0° to 5° with a step size of 0.001°. To improve the angular resolution, 2.5° Soller slits were used at both the incident and the receiving sides. In addition, an incident slit of width 0.10 mm and two receiving slits of width 0.20 mm each were used. The momentum transfer along the thin film surface normal, z, is given by the scattering wave vector transfer, $Q_z \equiv \frac{4\pi}{\lambda}\sin\theta$, where θ is the incidence angle. Postmeasurement, the reflectivity, R, footprint-corrected[63] and plotted as a function of Q_z, revealed multiple equispaced oscillations known as Kiessig fringes. These fringes arose due to the interference of the X-rays reflected from different interfaces, primarily the top (between the air and the film) and the bottom (between the film and the substrate). To determine the film thickness, d, the XRR data were fit using the GenX[64] software. The d values were also estimated directly using $d \equiv \frac{2\pi}{\Delta Q_z}$, where ΔQ_z is the period of the oscillation in the reflectivity curve (i.e., the difference in Q_z between the minima or maxima of consecutive Kiessig fringes). To reduce the error in the estimation of the film thickness to the extent possible, the d value was determined using the average ΔQ_z obtained from as many fringes in the reflectivity profile as was practicable.

RESULTS AND DISCUSSION

We performed SE measurements on thin films of PS and chitosan of several thicknesses. As the films were optically transparent (see Figure S4, Supporting Information) in the range of wavelengths investigated, we used the Cauchy dispersion equation, eq 2, to fit the measured SE data. In general, polymer thin films prepared by spin coating can be modeled as either optically isotropic or anisotropic. As polymer thin films typically exhibit in-plane optical isotropy, it is expected that the exhibited anisotropy is uniaxial.[24,30,33] Therefore, it was sufficient to model anisotropic films as being uniaxially anisotropic.

In the past, ellipsometry measurements were performed at a single AOI typically near, but not at, the Brewster's angle of the thin film. This can be understood by considering the sensitivity of the measurement using $\delta\Delta$, defined as the difference in the measured or simulated value of Δ for two different thin films

https://doi.org/10.1021/acs.langmuir.4c01761
Langmuir 2024, 40, 14153−14165

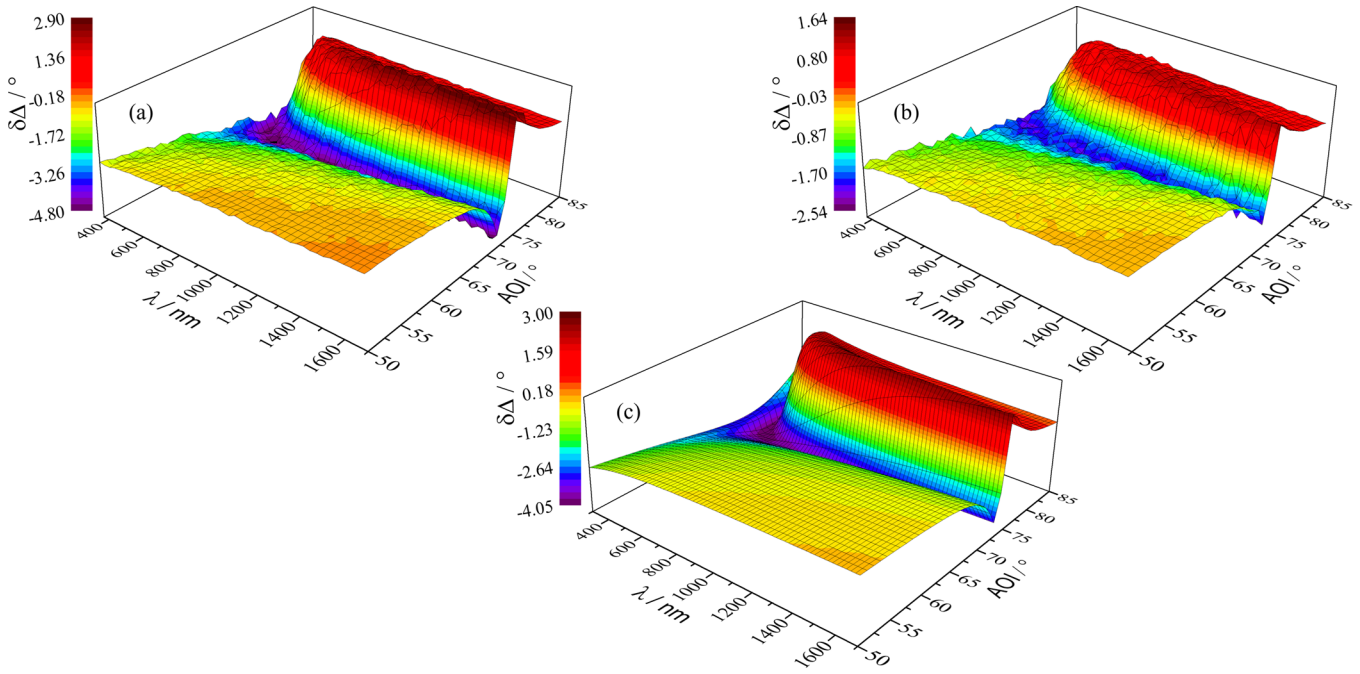

Figure 1. Sensitivity, $\delta\Delta$, of the measured ellipsometric angle Δ as a function of AOI and incident wavelength, λ, for a change in the film thickness of (a) 1 nm (PS, experimental data), (b) 0.84 nm (chitosan, experimental data), and (c) 1 nm (PS, simulated data).

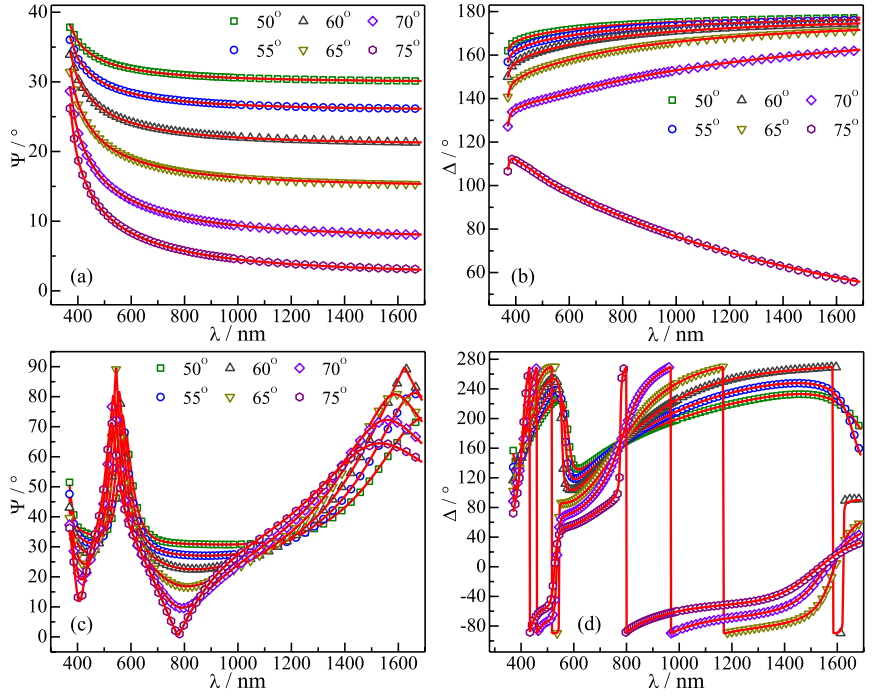

Figure 2. Dependence of Ψ and Δ on λ for PS films of thickness 12 nm, (a) and (b), and 310 nm, (c) and (d). Data (hollow symbols) acquired at multiple AOI ranging from 50° to 75° are shown. The solid curves represent the simultaneous fits of the experimental data using the optically isotropic model.

whose thickness differed by a certain value, which in our case was close to 1 nm. From Figure 1, it can be seen that the change in $\delta\Delta$ upon varying the AOI and the λ of the incident radiation was rather large close to the minimum. This explains the necessity of performing preparatory measurements to determine the appropriate AOI and the incident λ at which the Ψ and Δ exhibit adequate sensitivity to changes in the thin film thickness and the refractive index.[17,29,39−41,48,65] By performing ellipsometry measurements at multiple AOI and λ, which are straightforward using VASE, such preparatory measurements are rendered unnecessary.[39,56] This can be especially helpful when investigating uniaxial anisotropy in polymer thin films.[26−31] In addition, multiple angle measurements enable the resolution of the periodicity problem that arises in the determination of thin film thickness using ellipsometry[9,48] and the reduction in the correlation between the values for the film thickness and the refractive index obtained by fitting the ellipsometry data.[48] From Figure 1, it can also be seen that

https://doi.org/10.1021/acs.langmuir.4c01761
Langmuir 2024, 40, 14153−14165

Table 1. Film Thickness, RMSE, and Refractive Indices (n_{iso}, n_{xy}, and n_z) of PS Films Obtained using the Isotropic and the Anisotropic Models[a]

isotropic			uniaxial Anisotropic				
thickness/nm	RMSE	n_{iso}	thickness/nm	RMSE	n_{xy}	n_z	$\Delta n \equiv n_{xy} - n_z$
12	0.695	1.685	8	0.549	1.704	1.979	−0.275
18	1.146	1.635	13	0.903	1.613	1.817	−0.204
27	0.834	1.587	25	0.686	1.579	1.652	−0.073
42	0.873	1.582	42	0.739	1.575	1.583	−0.008
63	2.446	1.583	63	2.116	1.572	1.581	−0.009
99	2.514	1.582	99	1.675	1.580	1.587	−0.007
122	3.343	1.584	122	2.561	1.584	1.590	−0.006
140	5.389	1.586	140	5.274	1.586	1.589	−0.003
192	5.256	1.585	192	5.198	1.585	1.585	0.000
242	7.564	1.590	242	7.247	1.590	1.589	0.001
310	7.752	1.586	310	7.225	1.585	1.584	0.001

[a]Parameter values were determined by simultaneously fitting the λ dependence of Ψ and Δ obtained at multiple AOI. The n values correspond to $\lambda \approx 633$ nm. As a measure of the optical anisotropy, the Δn has also been provided.

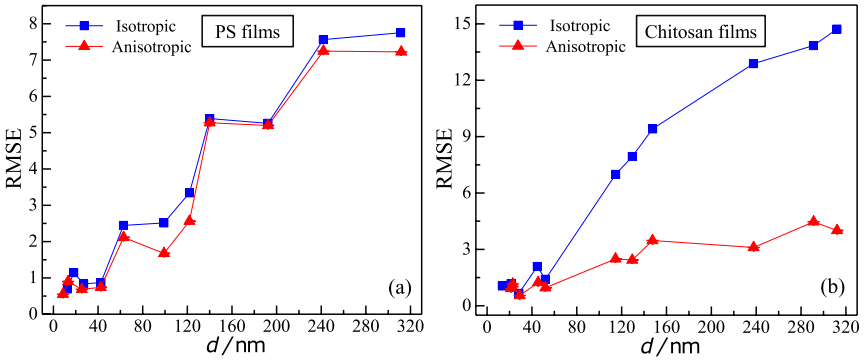

Figure 3. Dependence of RMSE on d for thin films of PS (a), and chitosan (b). The RMSE values were obtained from simultaneous fits of the λ dependence of Ψ and Δ at multiple AOI using optically isotropic (blue squares) and anisotropic (red triangles) models. The solid lines between the data points are intended as a guide to the eye.

while the range of the variation in $\delta\Delta$ exhibited some dependence on the particular polymer under consideration, the experimental data for PS (a) and chitosan (b) and the simulated data for PS (c) look qualitatively similar. Finally, simultaneous fits to SE data from multiple AOI can provide better estimates for the fit parameters. The variation of the film thickness determined at each AOI, D, as a function of AOI for PS of thickness 12, 18, 27, and 310 nm and for chitosan of thickness 13, 28, 238, and 312 nm is shown in Figures S5 and S6 of the Supporting Information. As can be seen from the figures, D exhibited a weak dependence on AOI. The variation in D for the different AOI used in this work was significantly smaller than the surface roughness of the film as determined by XRR (see Figure 7 and the accompanying discussion). Unsurprisingly, the film thickness determined by simultaneously fitting the SE data for several AOI, d, has an associated error that is generally smaller than that for D.

Our discussion hereon makes exclusive use of results obtained through the simultaneous fitting of ellipsometry data obtained at multiple AOI. We begin with an examination of PS thin films of several thicknesses between 12 and 310 nm. Figure 2 displays the λ dependence of Ψ and Δ for the thinnest (12 nm) and the thickest (310 nm) thin films. These values of the film thickness were determined by using the isotropic model to fit the ellipsometry data. Even a quick glance at Figure 2 suggests that fits of adequate quality can be obtained at all of the measured AOI using the isotropic model for both of the thin films whose thicknesses vary by over an order of magnitude. The fit parameters, i.e., the thickness and the refractive indices, obtained using the isotropic and the anisotropic model fits and the corresponding RMSE values are summarized in Table 1. Note that the RMSE values from the fits to the two models are comparable, with no apparent improvement upon using the anisotropic model, which employs a greater number of fitting parameters. A comparison of the variation of RMSE with the thin film thickness, d, is displayed in Figure 3a. Note that the minimum RMSE tends to increase with d, a trend also observed in prior work.[24] A brief discussion of the tendency of RMSE to exhibit an increase with increasing d is provided in the Supporting Information.

A similar examination was performed on several chitosan thin films whose thicknesses were between 13 and 312 nm. Figure 4 displays the λ dependence of Ψ and Δ for the thinnest (13 nm) and the thickest (312 nm) chitosan thin films. For the 13 nm thin film, fits of adequate quality were obtained at all AOI using the isotropic model. However, for $d \geq 30$ nm, the anisotropic model performed significantly better at all AOI. For the 312 nm thin film, the fits to the anisotropic model are shown in Figure 4c,d. Note that the values of the film thickness provided here were determined using the isotropic model to fit the ellipsometry data, as both the models yielded nearly identical d values for films with thicknesses typically exceeding 30 nm. Similarly to the PS thin films, a summary of the fit parameters and the corresponding RMSE values are provided

https://doi.org/10.1021/acs.langmuir.4c01761
Langmuir 2024, 40, 14153−14165

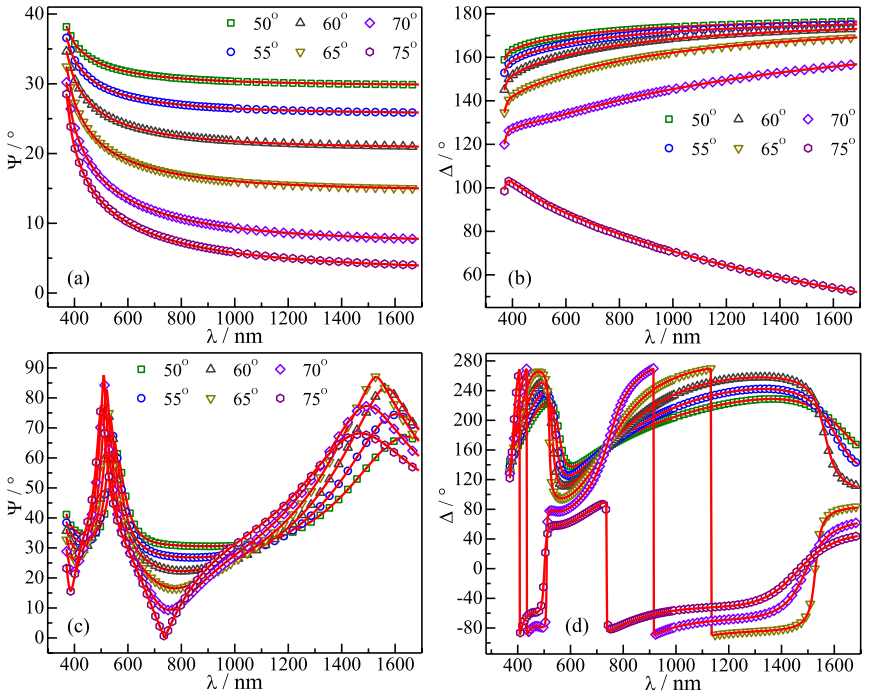

Figure 4. Dependence of Ψ and Δ on λ for chitosan thin films of thickness 13 nm, (a) and (b), and 312 nm, (c) and (d). Data (hollow symbols) acquired at multiple AOI ranging from 50° to 75° are shown. The solid curves in (a) and (b) represent the simultaneous fits of the experimental data using the optically isotropic model, while those in (c) and (d) correspond to fits using the optically anisotropic model.

Table 2. Film Thickness, RMSE, and Refractive Indices (n_{iso}, n_{xy}, and n_z) of Chitosan Films Obtained using the Isotropic and the Anisotropic Models[a]

isotropic			uniaxial Anisotropic				
thickness/nm	RMSE	n_{iso}	thickness/nm	RMSE	n_{xy}	n_z	$\Delta n \equiv n_{xy} - n_z$
13	1.054	1.594	21	0.923	1.508	1.299	0.209
21	1.170	1.584	23	1.160	1.571	1.517	0.054
28	0.660	1.528	29	0.543	1.530	1.506	0.024
45	2.089	1.531	45	1.237	1.534	1.516	0.018
52	1.409	1.527	52	0.957	1.537	1.518	0.019
115	6.989	1.527	115	2.494	1.530	1.512	0.018
129	7.942	1.530	129	2.432	1.531	1.514	0.017
147	9.411	1.530	147	3.473	1.532	1.513	0.019
238	12.883	1.530	238	3.102	1.531	1.511	0.020
291	13.846	1.534	291	4.466	1.534	1.517	0.017
312	14.720	1.529	312	4.006	1.530	1.513	0.017

[a]Parameter values were determined by simultaneously fitting the λ dependence of Ψ and Δ obtained at multiple AOI. The n values correspond to $\lambda \approx 633$ nm. As a measure of the optical anisotropy, the Δn has also been provided.

in Table 2. A comparison of the variation of RMSE with the thin film thickness, d, is displayed in Figure 3b. In contrast to PS films (see Table 1), the RMSE values from the fits to the two models are comparable only for $d \leq 30$ nm. For the thicker films, the RMSE values from the fits to the anisotropic model were appreciably smaller when compared to those from the isotropic model. For instance, for a chitosan film of thickness 45 nm, the RMSE decreased from approximately 2.1 (isotropic) to approximately 1.2 (anisotropic).

While the isotropic model and the anisotropic models yielded similar minimum RMSE values for each of the investigated PS film thicknesses, the obtained d values noticeably disagreed for the thinner films ($d \leq 30$ nm, see Table 1). For instance, for the same thin film, the isotropic model yielded d = 12 nm, while the anisotropic model yielded d = 8 nm. It is germane to note that the difference in the obtained d is significantly larger than the error expected in SE measurements. Similarly, from Table 2, it is clear that a larger discrepancy in the d values was observed for the thinnest chitosan film. Here, the isotropic model yielded d = 13 nm, while the anisotropic model yielded d = 21 nm.

For PS thin films, the variation of RMSE upon varying the fit parameter corresponding to the thickness, t, shown in Figure 5 suggests a reason for the discrepancy in the d values obtained from the isotropic and anisotropic model fits. As can be seen in Figure 5, the isotropic model demonstrates a well-defined minimum associated with a unique d value. This minimum corresponds to the d value returned by the CompleteEASE program following the fit to the isotropic model. In contrast, for anisotropic model fits, the RMSE exhibits little variation across a range of t values, resulting in a relatively shallow minimum. For instance, in Figure 5a, the RMSE for the

https://doi.org/10.1021/acs.langmuir.4c01761
Langmuir 2024, 40, 14153−14165

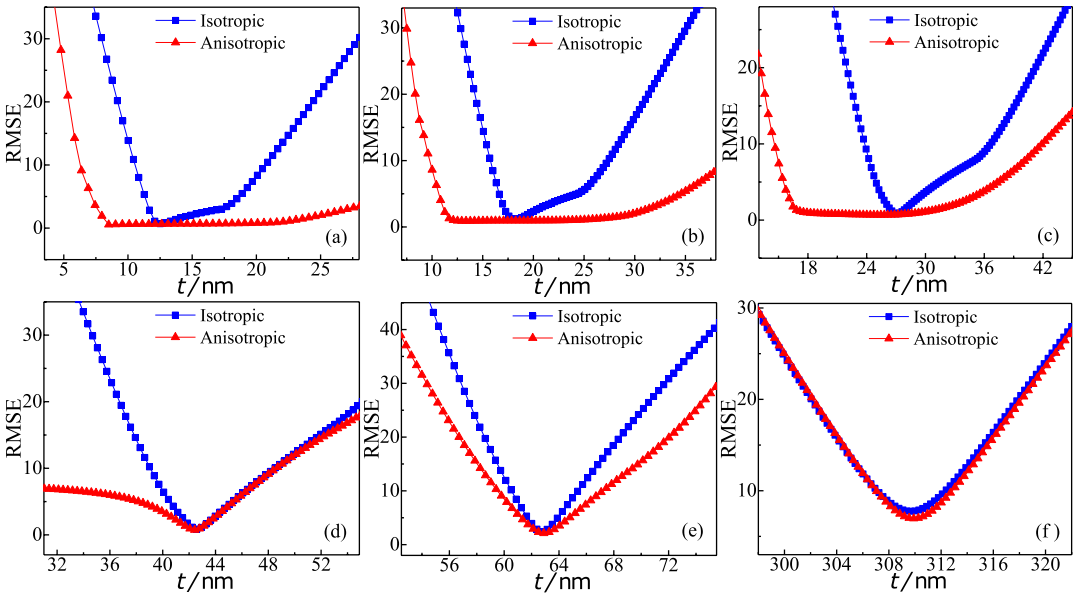

Figure 5. Variation of RMSE upon varying the value of the fit parameter corresponding to the thickness, *t*, for PS films of thickness 12 nm (a), 18 nm (b), 27 nm (c), 42 nm (d), 63 nm (e), and 310 nm (f). The RMSE values were obtained from simultaneous fits of the λ dependence of Ψ and Δ at multiple AOI using optically isotropic (blue squares) and anisotropic (red triangles) models.

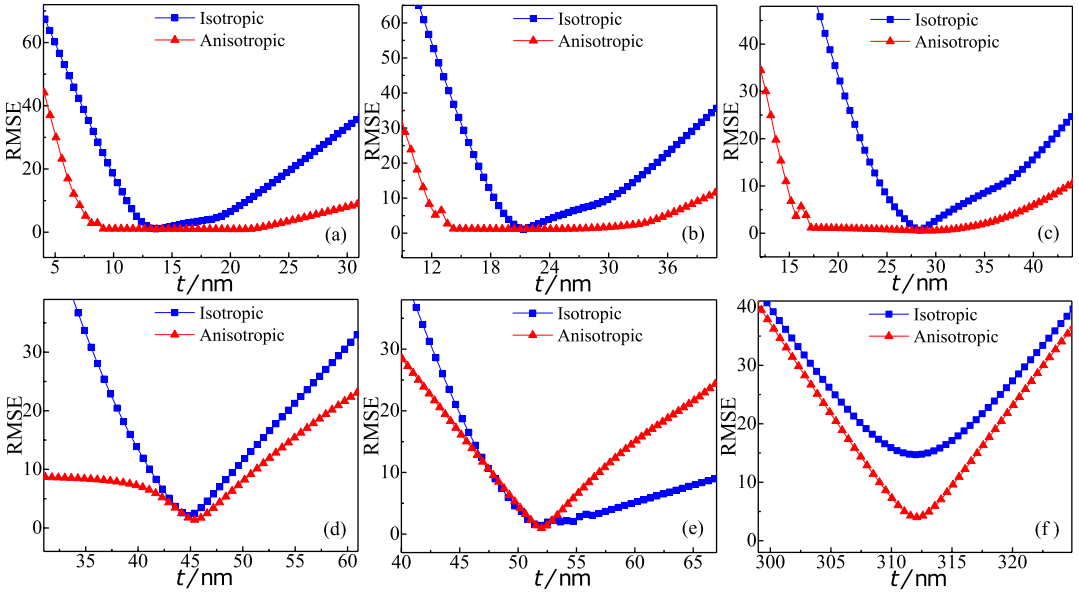

Figure 6. Variation of RMSE upon varying the value of the fit parameter corresponding to the thickness, *t*, for chitosan films of thickness 13 nm (a), 21 nm (b), 28 nm (c), 45 nm (d), 52 nm (e), and 312 nm (f). The RMSE values were obtained from simultaneous fits of the λ dependence of Ψ and Δ at multiple AOI using optically isotropic (blue squares) and anisotropic (red triangles) models.

isotropic model fit exhibits a clear minimum near d = 12 nm, while the RMSE for the anisotropic model fit exhibits little variation between 8 and 21 nm. We believe that the shallow minimum made the identification of a unique d value challenging and contributed to the observed discrepancy in the d value returned by the CompleteEASE program from fits to the isotropic and anisotropic models. As can be seen from Figure 5d,e,f, the situation significantly improves for $d \geq 42$ nm, where a reasonably well-defined minimum in the RMSE can be identified when using either of the two models to fit the data. This similarity results in the d value returned by the CompleteEASE program by fitting to either model being nearly identical. Additionally, as can be seen from Figure 5, the RMSE values for $d \geq 42$ nm films from anisotropic model fits clearly do not exceed those from isotropic model fits over a range of t values. For d = 310 nm, there is little difference in the RMSE values obtained from either of the model fits. For the chitosan films, the observed trend is similar to that for the PS thin films discussed above (see Figure 6). However, for the d = 312 nm chitosan film, the anisotropic model yielded a discernably lower RMSE value compared to that obtained from the isotropic model. This difference may be related to the significantly larger anisotropy exhibited by the chitosan thin films[24,31] compared to PS thin films of similar thickness[42] and also to micrometer thick PS films.[35−37] The larger anisotropy in chitosan thin films is typically attributed to the dominant polarizable groups being located in the chain backbone[24,31] as opposed to in the side chains[36,37] as is the case for PS.

https://doi.org/10.1021/acs.langmuir.4c01761
Langmuir 2024, 40, 14153−14165

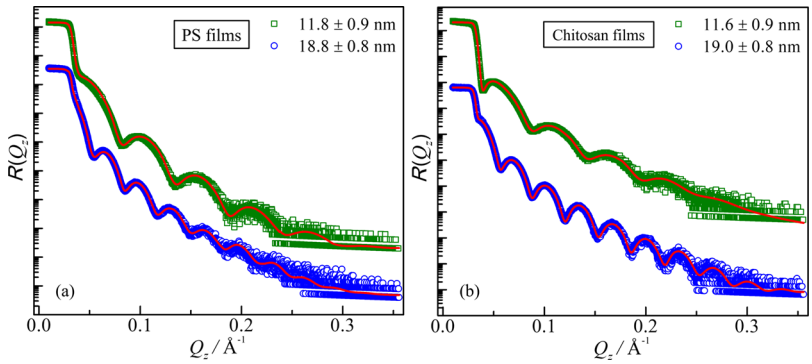

Figure 7. (a) Dependence of reflectivity, $R(Q_z)$, on the normal scattering vector, Q_z, for PS thin films for $d \approx 11.8 \pm 0.9$ nm (green squares) and $d \approx 18.8 \pm 0.8$ nm (blue circles). The thickness values were derived from the fits (solid red curves) and agree with those determined by fitting the SE data using the isotropic model. (b) Dependence of reflectivity, $R(Q_z)$, on the normal scattering vector, Q_z, for chitosan thin films for $d \approx 11.6 \pm 0.9$ nm (green squares) and $d \approx 19.0 \pm 0.8$ nm (blue circles). The thickness values were derived from the fits (solid red curves) and agree with those determined by fitting the SE data using the isotropic model.

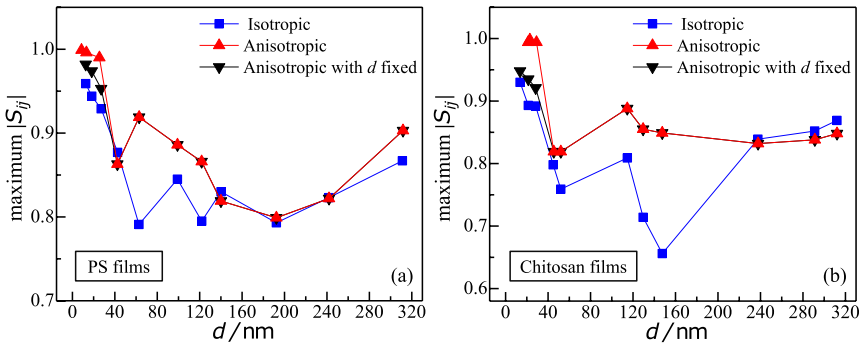

Figure 8. Dependence of the maximum absolute value of the correlation coefficient, maximum $|S_{ij}|$, on d for thin films of PS (a) and chitosan (b). The correlation coefficients were obtained using simultaneous fits of the λ dependence of Ψ and Δ at multiple AOI to the following models: optically isotropic (blue squares), uniaxially anisotropic (upward red triangles), and uniaxially anisotropic while holding d fixed (downward black triangles).

For the thinnest PS film, the thickness obtained from the anisotropic model differed by approximately 30% from that obtained using the isotropic model. The relative discrepancy was even more significant, reaching nearly 54%, for the thinnest chitosan film. This naturally prompts the question of which, if any, of the two thickness values obtained by fitting the SE data provides a reasonably accurate estimate for the thin film thickness. To address this, we determined the film thickness of the two thinnest films each of PS and chitosan using XRR. The reflectivity, $R(Q_z)$, as a function of the out-of-plane scattering vector, Q_z, for the two thinnest PS films is provided in Figure 7a. The model employed for the fits to the XRR data included a 1.15 nm native SiO_2 layer (determined from SE) above the Si substrate and a uniform layer of PS on top of that. Fitting the XRR data yielded film thicknesses of 11.8 ± 0.9 and 18.8 ± 0.8 nm. As already mentioned in the experimental section, the obtained thicknesses exhibited excellent agreement with that obtained using the peak separation of the Kiessig fringes. The thicknesses of the two thin films obtained using XRR (11.8 ± 0.9 and 18.8 ± 0.8 nm) were rather close to the corresponding thicknesses obtained using the isotropic fits to the SE data (12 and 18 nm). For the two thinnest chitosan films, the reflectivity, $R(Q_z)$, as a function of the out-of-plane scattering vector, Q_z, is shown in Figure 7b. While the arrangement of the layers included in the model was similar to that for the PS, the model employed a 2 nm native SiO_2 layer (determined from SE) above the Si substrate and a uniform layer of chitosan on top. Fitting the XRR data yielded film thicknesses of 11.6 ± 0.9 and 19.0 ± 0.8 nm. The thicknesses of the two thin films obtained using XRR (11.6 ± 0.9 and 19.0 ± 0.8 nm) were close to the corresponding thicknesses obtained using the isotropic fits to the SE data (13 and 21 nm). The discussion above suggests that for both the PS and the chitosan thin films, the isotropic model fits to the SE data yielded a more accurate value for the film thickness.

For the thinnest films, it is noteworthy that Table 1 reveals significantly larger values for the anisotropic refractive indices, n_{xy} and n_z, compared to the corresponding values for the thicker films. From Figure S7 in the Supporting Information, it is evident that the variation of the RMSE with n was qualitatively similar, including the presence of a shallow minimum, to the variation of RMSE with t (Figure 5). First, the dependence of RMSE on the isotropic refractive index, n_{iso}, exhibited a clear, well-defined minimum. In contrast, the dependence of RMSE on the anisotropic refractive indices, n_{xy} and n_z, exhibited a minimum that was broad and shallow. As indicated in Table 1, the n_z for the $d = 12$ nm film obtained from the anisotropic fit appears to be rather large and may be unphysical. As a consequence, the corresponding Δn was also rather large. For instance, while Δn was 0.001 for the 310 nm film, it reached −0.275 for the 12 nm film. For $d \leq 30$ nm chitosan thin films, on the other hand, either the n_{xy} or the n_z or both were smaller than that for the thicker films. As can be

https://doi.org/10.1021/acs.langmuir.4c01761
Langmuir 2024, 40, 14153−14165

Table 3. Film Thickness, RMSE, and Refractive Indices (n_{iso}, n_{xy}, and n_z) of PS Films Obtained using the Optically Isotropic and the Optically Anisotropic Models[a]

isotropic			uniaxial Anisotropic				
thickness/nm	RMSE	n_{iso}	thickness/nm	RMSE	n_{xy}	n_z	$\Delta n \equiv n_{xy} - n_z$
12	0.695	1.685	12	0.647	1.663	1.673	-0.010
18	1.146	1.635	18	0.949	1.589	1.596	-0.007
27	0.834	1.587	27	0.726	1.571	1.579	-0.008

[a]Parameter values were determined by simultaneously fitting the λ dependence of Ψ and Δ obtained at multiple AOI. The n values correspond to $\lambda \approx 633$ nm. As a measure of the optical anisotropy, the Δn has also been provided. While performing the fits using the anisotropic model, the thickness determined from the isotropic model was used as the input value and held fixed to determine the refractive indices, n_{xy} and n_z. The obtained Δn values for the ultrathin films were closer to those determined for the thicker films shown in Table 1.

seen from Figure S8, the RMSE dependence on n and t for chitosan exhibited features similar to that described above for PS thin films, including the presence of a shallow minimum. From Table 2, it can be seen that for the $d = 13$ nm film, the n_z obtained from the anisotropic fit was comparatively smaller. As a consequence, the corresponding Δn was rather large, perhaps unphysically so. For instance, while Δn was 0.017 for the 312 nm film, it reached 0.209 for the 13 nm film.

Moreover, akin to the earlier observations for PS films, this limitation of the anisotropic model in accurately determining d is consistent with the values obtained for the correlation coefficient, S_{ij}. This can be understood by considering the behavior of the absolute value of the correlation coefficient, $|S_{ij}|$, as a function of d. The maximum value of $|S_{ij}|$ as a function of d obtained from both models is shown in Figure 8. As can be seen from the figure, for $d \leq 30$ (ultrathin films) and in contrast to the thicker films, the $|S_{ij}|$ values of the anisotropic model approach 1 and are larger when compared to the isotropic case. Such $|S_{ij}|$ values indicate a strong correlation between d and n and are behind the limited ability of the data fits to uniquely determine the two parameters in the case of ultrathin films. As mentioned earlier, in such cases, it becomes necessary to independently determine d and n for the anisotropic model fitting. Note that the maximum $|S_{ij}|$ decreased when d was used as a fixed input parameter in the fits to the anisotropic model (Figure 8). This point will be discussed further below.

To summarize the above discussion, for $d \leq 30$ nm, the thickness obtained by fitting the SE data to the anisotropic model disagreed with that obtained by fitting to the isotropic model and to that obtained from XRR. Additionally, for these thin films, the values of n_z obtained from the fits were either notably large (for PS) or small (for chitosan), potentially reaching unphysically extreme values. For ultrathin films, a strong correlation between the d and n has been reported in the literature.[18,33,48,52] For such thin polymer films, in addition, past literature has demonstrated that a small increment in the thickness resulted in a significant change in the refractive index obtained from the fit.[48] Therefore, to better understand the aforementioned observations for the $d \leq 30$ nm films, we carefully considered the correlation matrix of the fit parameters, in particular the correlation coefficient, S_{ij}, between d and the parameter A_z from the Cauchy equation, eq 2, for n_z. For $d \leq 30$ nm thin films, the $|S_{ij}|$ between d and A_z from the anisotropic model was close to 1 and the largest among the elements of the correlation matrix. This suggested that one of these two parameters was redundant and could be the reason behind the rather broad, shallow minimum seen in Figures 5 and 6. Upon increasing the film thickness, the correlation between these parameters weakens. This can be seen from Figure 8 which shows that the value of the largest $|S_{ij}|$ tends to decrease with increasing d. The decrease in $|S_{ij}|$ is consistent with the tendency of the t dependence of RMSE to transition from exhibiting a broad, shallow minimum to a sharp, well-defined one. As an illustration, the correlation matrix for the fit parameters for the 21 nm chitosan film is provided in Table S1 of Supporting Information.

The existence of significant correlations between d and n for $d \leq 30$ nm may raise concerns about the reliability of parameter values derived from fitting SE data. The situation, however, is not as bleak. As discussed earlier, the d values obtained from fits to the isotropic model consistently corresponded to a well-defined minimum. This held true not only for the PS films but also for the chitosan films. More importantly, the obtained d values exhibited excellent agreement with the film thickness determined using XRR. Previous studies have pointed out that the anisotropy in chitosan films[24,31] is significantly larger compared to that in PS films[42] of similar thickness. This suggested that the film thickness can be reliably determined by fitting the SE data to the isotropic model, even when the film exhibited significant optical anisotropy. Additionally, for the PS films, the n_{iso} values obtained are consistent with those reported in the literature.[18,37,42,66]

For thin films with $d \leq 30$ nm, the determination of the in-plane, n_{xy}, and out-of-plane, n_z, refractive indices needs more careful consideration. In the case of PS, it can be seen from Table 1 that either n_{xy} or n_z or both are significantly larger than the corresponding n_{iso}. More worryingly, the $|\Delta n|$ is also unreasonably large. However, in the case of chitosan, Table 2 suggests that either n_{xy} or n_z or both are significantly smaller than the corresponding n_{iso}. As discussed earlier, even though we expect chitosan films to exhibit a larger anisotropy than PS, the value of $|\Delta n|$ is perhaps unreasonably large in this case too. These observations indicate that the direct application of the anisotropic model for fitting SE data has severe limitations. In the subsequent discussion, we will provide an alternate approach that can at least mitigate some of the issues associated with using the anisotropic model to fit SE data.

We have already indicated that the large values of the correlation coefficients obtained while using the anisotropic model to fit the SE data could be behind the unreasonable values of the parameters obtained from the fit. We have also established earlier that the film thickness obtained by fitting the SE data with the isotropic model yielded reliable values for the film thickness. Therefore, we propose the following: use the d determined by fitting to the isotropic model as an input parameter and hold it fixed and fit the SE data to the anisotropic model to determine n_{xy} and n_z. The results obtained using such a fitting procedure are summarized in

https://doi.org/10.1021/acs.langmuir.4c01761
Langmuir 2024, 40, 14153−14165

Table 4. Film Thickness, RMSE, and Refractive Indices (n_{iso}, n_{xy}, and n_z) of Chitosan Films Obtained using the Optically Isotropic and the Optically Anisotropic Models[a]

isotropic			uniaxial Anisotropic				
thickness/nm	RMSE	n_{iso}	thickness/nm	RMSE	n_{xy}	n_z	$\Delta n \equiv n_{xy} - n_z$
13	1.054	1.594	13	1.043	1.591	1.566	0.025
21	1.170	1.584	21	1.163	1.578	1.554	0.024
28	0.660	1.528	28	0.543	1.530	1.509	0.021

[a]Parameter values were determined by simultaneously fitting the λ dependence of Ψ and Δ obtained at multiple AOI. The n values correspond to $\lambda \approx 633$ nm. As a measure of the optical anisotropy, the Δn has also been provided. While performing the fits using the anisotropic model, the thickness determined from the isotropic model was used as the input value and held fixed to determine the refractive indices, n_{xy} and n_z. The obtained Δn values for the ultrathin films were closer to those determined for the thicker films shown in Table 2.

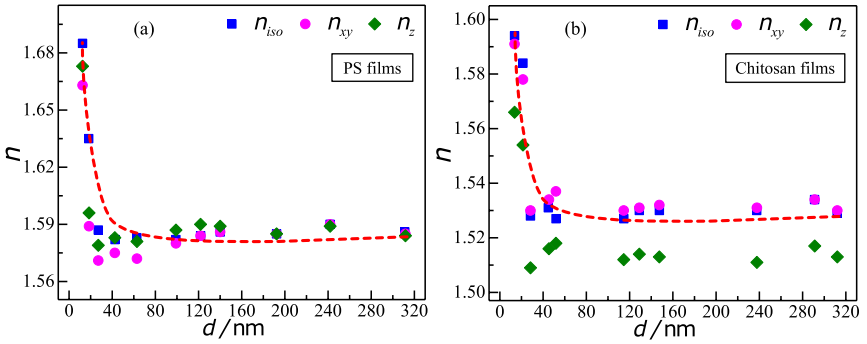

Figure 9. Dependence of the refractive indices on d for thin films of PS (a) and chitosan (b). The refractive index determined using the optically isotropic model, n_{iso} (blue squares), along with the in-plane, n_{xy} (magenta circles), and the out-of-plane, n_z (green diamonds), refractive indices determined using the optically anisotropic model are shown. For ultrathin films, $d \leq 30$ nm, the anisotropic refractive indices, n_{xy} and n_z, were determined using d value determined from the fits to the isotropic model as a fixed input parameter. The dashed curves are merely to guide the eye.

Tables 3 and 4. Note that each step of the two-step fitting procedure utilizes the same number of effective fit parameters: d and n_{iso} in the first step and n_{xy} and n_z in the second. Therefore, the reduction in RMSE of 1−18% is not a consequence of an increase in the number of effective fit parameters. The n_{xy} and n_z values for both PS and chitosan thin films are significantly closer to n_{iso} when compared to the values in Tables 1 and 2, respectively. More interestingly, the Δn values in Tables 3 and 4 appear to be more reasonable and that the chitosan films exhibit a significantly larger optical anisotropy. A reason for this significant improvement can perhaps be traced to the weakening of the correlation between the fit parameters. The correlation matrices for the fit parameters for the 21 nm chitosan film are provided in Tables S1 and S2 of the Supporting Information. For instance, while fitting the SE data for the 21 nm chitosan film using the anisotropic model, the most significant correlation was found to be between d and A_z with a correlation coefficient of −0.998 (see Table S1). Upon fitting to the anisotropic model while holding d fixed, the most significant correlation was found between A_z and B_z and the correlation coefficient was −0.935 (see Table S2). In addition, with the modified fitting procedure, the variation of RMSE with n_{iso}, n_{xy}, and n_z exhibited a well-defined minimum for both PS (Figure S9) and chitosan (Figure S10) thin films. The refractive indices obtained from such well-defined minima appear to be more reasonable than the values in Tables 1 and 2 which were obtained by simultaneously fitting all the parameters in the anisotropic model.

The dependence on d of n_{iso}, n_{xy}, and n_z determined using the modified fitting procedure is provided in Figure 9. It can be seen that the n_{iso}, n_{xy}, and n_z exhibit a rapid decrease with an increase in d. Upon further increase in d, all of the refractive indices essentially show little variation. The thickness dependence and the obtained refractive indices are consistent with past literature for both films of PS[18,37,42,66] and chitosan.[24,31] The variation of Δn is shown in Figure 10. These Δn values for

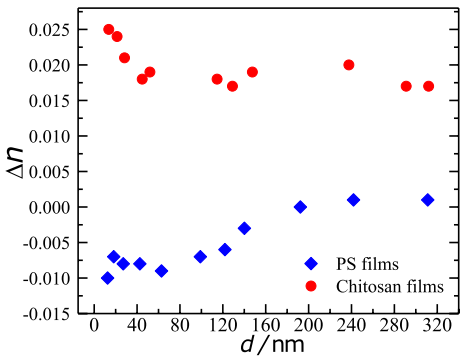

Figure 10. Variation of Δn with d for PS (blue diamonds) and chitosan (red circles) thin films. As can be seen, the Δn for PS is negative or close to zero, while that for chitosan is clearly positive.

PS thin films are close to 0 but slightly negative and agree well with that from past literature.[35−37,42] As $\Delta n \approx 0$ for the PS thin films, they were nearly isotropic. This is consistent with the fact that very little decrease in the RMSE was observed during the second step in the two-step fitting procedure, i.e., upon using the anisotropic model while holding d fixed to the value obtained from the first step. In contrast, the Δn values for the chitosan films obtained from the modified fits were positive and consistent with earlier results.[24,31] Note that past literature has almost exclusively utilized the isotropic model to fit SE data from PS films.[16,40,42,51] Such a choice can now be

https://doi.org/10.1021/acs.langmuir.4c01761
Langmuir 2024, 40, 14153−14165

rationalized by noting that the Δn for PS was approximately an order of magnitude smaller than that for the chitosan thin films (refer Tables 3 and 4 and Figure 10).

CONCLUSIONS

Previous studies have shown that the sensitivity of ellipsometry in determining film thickness and refractive index depends on the wavelength of electromagnetic radiation and the AOI. Achieving the desired sensitivity often requires extensive experimentation with various wavelength and incidence angle combinations. Using a spectroscopic ellipsometer with variable incidence angles can eliminate the need for such optimization. Simultaneous fitting of data from multiple angles generally yields smaller error values for thickness compared to fitting data from individual angles. In this work, we systematically compared the fits over a range of wavelengths using the isotropic and the anisotropic models for PS and chitosan thin films of several thicknesses. For both sets of thin films and for $d \leq 30$ nm, we found a significant difference in the film thickness obtained from the isotropic and the anisotropic models. To determine the reliability of the obtained thickness values, we also determined the film thickness using XRR. For both PS and chitosan thin films, the film thickness obtained from XRR was close to that obtained by fits to the isotropic model. This suggested that, even in the presence of optical anisotropy, the film thickness can be reliably determined using fits to the isotropic model. However, the obtained refractive indices, on the other hand, especially from the anisotropic model, were either relatively too large or too small.

For thin films with $d \leq 30$ nm, the dependence of the RMSE on each parameter of the anisotropic model (film thickness and the two refractive indices) exhibited a wide, shallow minimum. This phenomenon can be tied to the strong correlations, as evidenced by the maximum absolute correlation coefficient being close to 1, between certain fit parameters in the case of the thinnest films. The diminished reliability of the thickness and the refractive indices obtained using the anisotropic model fits can be attributed to these strong correlations.

Given that the thickness obtained by fits to the isotropic model has proven reliable, one way to improve the reliability of the refractive indices obtained by fits to the anisotropic model is as follows. While performing fits using the anisotropic model, set the thickness of the thin film to that obtained from the fits to the isotropic model and hold it fixed. Now perform the fit only for the parameters related to the two refractive indices. The n_{xy}, n_z, and Δn obtained by using such a fitting procedure appear to be significantly more reasonable and consistent with the data for the thicker films and the existing literature. Improvements in the reasonableness of the fit parameter values were accompanied by a decrease in the maximum value of the absolute correlation coefficient between any two of the fit parameters. Needless to add, the dependence of the RMSE on the refractive indices displayed a clear, well-defined minimum, enabling the identification of unique values for the fit parameters.

In conclusion, accurately determining refractive indices in ultrathin films with uniaxial anisotropy has been challenging due to strong correlations between the fit parameters in the anisotropic model. In this work, we have proposed an approach using which reliable values can be obtained for the refractive indices and the optical anisotropy even for ultrathin films using *only* spectroscopic ellipsometry data.

ASSOCIATED CONTENT

Supporting Information

The Supporting Information is available free of charge at https://pubs.acs.org/doi/10.1021/acs.langmuir.4c01761.

Description of root mean squared error (RMSE); absorbance spectra for PS and chitosan films; thickness as a function of angle of incidence for PS and chitosan films; variation of RMSE with refractive index, n for PS and chitosan films with thickness (d) as a fit parameter; correlation matrices for a 21 nm thick chitosan film either with the d as a fit parameter or the d held fixed during fitting; and dependence of RMSE on n with d as fixed parameter for PS and chitosan films (PDF)

AUTHOR INFORMATION

Corresponding Authors

Sathish K. Sukumaran − *Graduate School of Organic Materials Science, Yamagata University, Yonezawa 992-8510, Japan*; Email: sa.k.sukumaran@gmail.com

Dillip K. Satapathy − *Soft Materials Laboratory, Department of Physics and Center for Soft and Biological Matter, IIT Madras, Chennai 600036, India*; orcid.org/0000-0002-3083-655X; Email: dks@iitm.ac.in

Author

Sonam Zangpo Bhutia − *Soft Materials Laboratory, Department of Physics and Center for Soft and Biological Matter, IIT Madras, Chennai 600036, India*; orcid.org/0009-0007-4151-6803

Complete contact information is available at: https://pubs.acs.org/10.1021/acs.langmuir.4c01761

Notes

The authors declare no competing financial interest.

ACKNOWLEDGMENTS

S.Z.B. acknowledges financial support from the Council of Scientific and Industrial Research and University Grants Commission (CSIR-UGC), Government of India. S.K.S. acknowledges financial support from the Japan Society for the Promotion of Science through Grant-in-Aid for Scientific Research (C) (19K03761 and 20K03876). D.K.S. acknowledges financial support from the Ministry of Education, Government of India, through the Scheme for Transformational and Advanced Research in Sciences (STARS) and the generous financial support from IIT Madras under the Institutes of Eminence (IoE) scheme.

REFERENCES

(1) Ouyang, J.; Chu, C.-W.; Szmanda, C. R.; Ma, L.; Yang, Y. Programmable polymer thin film and non-volatile memory device. *Nat. Mater.* **2004**, *3*, 918−922.

(2) Alcoutlabi, M.; McKenna, G. B. Effects of confinement on material behaviour at the nanometre size scale. *J. Phys.: Condens. Matter* **2005**, *17*, R461.

(3) Geethu, P.; Yadav, I.; Deshpande, S.; Aswal, V. K.; Satapathy, D. K. Soft confinement effects on dynamics of hydrated gelatin. *Macromolecules* **2017**, *50*, 6518−6528.

(4) Nygård, K.; Delcambre, S. P.; Satapathy, D. K.; Bunk, O.; Nealey, P. F.; van der Veen, J. F. Size-dependent shape evolution of patterned polymer films studied in situ by phase-retrieval-based small-angle X-ray scattering. *Macromolecules* **2012**, *45*, 5798−5805.

(5) Schubert, M.; Rheinländer, B.; Woollam, J. A.; Johs, B.; Herzinger, C. M. Extension of rotating-analyzer ellipsometry to generalized ellipsometry: determination of the dielectric function tensor from uniaxial TiO_2. *Journal of the Optical Society of America A* **1996**, *13*, 875−883.
(6) Johs, B.; Woollam, J. A.; Herzinger, C. M.; Hilfiker, J. N.; Synowicki, R. A.; Bungay, C. L. Overview of variable-angle spectroscopic ellipsometry (VASE): II. Advanced applications. *Opt. Metrol.: Crit. Rev.* **1999**, *10294*, 29−58.
(7) Woollam, J. A.; Hilfiker, J. N.; Tiwald, T. E.; Bungay, C. L.; Synowicki, R. A.; Meyer, D. E.; Herzinger, C. M.; Pfeiffer, G. L.; Cooney, G. T.; Green, S. E. Variable angle spectroscopic ellipsometry in the vacuum ultraviolet. In *Optical Metrology Roadmap for the Semiconductor, Optical, and Data Storage Industries*, 2000; Vol. *4099*, pp 197−205.
(8) Hilfiker, J. N.; Bungay, C. L.; Synowicki, R. A.; Tiwald, T. E.; Herzinger, C. M.; Johs, B.; Pribil, G. K.; Woollam, J. A. Progress in spectroscopic ellipsometry: Applications from vacuum ultraviolet to infrared. *J. Vac. Sci. Technol., A* **2003**, *21*, 1103−1108.
(9) Woollam, J. A.; Bungay, C. L.; Yan, L.; Thompson, D. W.; Hilfiker, J. N. Application of spectroscopic ellipsometry to characterization of optical thin films. In *Laser-Induced Damage in Optical Materials: 2002 and 7th International Workshop on Laser Beam and Optics Characterization*, 2003; pp 393−404.
(10) Langereis, E.; Heil, S.; Knoops, H. C.; Keuning, W.; Van de Sanden, M.; Kessels, W. In situ spectroscopic ellipsometry as a versatile tool for studying atomic layer deposition. *J. Phys. D: Appl. Phys.* **2009**, *42*, No. 073001.
(11) Burke, S. E.; Barrett, C. J. Swelling behavior of hyaluronic acid/polyallylamine hydrochloride multilayer films. *Biomacromolecules* **2005**, *6*, 1419−1428.
(12) Tan, W. S.; Cohen, R. E.; Rubner, M. F.; Sukhishvili, S. A. Temperature-induced, reversible swelling transitions in multilayers of a cationic triblock copolymer and a polyacid. *Macromolecules* **2010**, *43*, 1950−1957.
(13) Schubert, M. *Infrared ellipsometry on semiconductor layer structures: phonons, plasmons, and polaritons*; Springer Science & Business Media, 2004; Vol. *209*.
(14) Elwing, H. Protein absorption and ellipsometry in biomaterial research. *Biomaterials* **1998**, *19*, 397−406.
(15) Pradipkanti, L.; Satapathy, D. K. Water desorption from a confined biopolymer. *Soft Matter* **2018**, *14*, 2163−2169.
(16) Pradipkanti, L.; Chowdhury, M.; Satapathy, D. K. Stratification and two glass-like thermal transitions in aged polymer films. *Phys. Chem. Chem. Phys.* **2017**, *19*, 29263−29270.
(17) Keddie, J. L.; Jones, R. A.; Cory, R. A. Size-dependent depression of the glass transition temperature in polymer films. *Europhys. Lett.* **1994**, *27*, 59.
(18) Vignaud, G.; Chebil, M. S.; Bal, J.; Delorme, N.; Beuvier, T.; Grohens, Y.; Gibaud, A. Densification and depression in glass transition temperature in polystyrene thin films. *Langmuir* **2014**, *30*, 11599−11608.
(19) Pradipkanti, L.; Satapathy, D. K. Effect of bimodal molecular weight distribution on glass transition of confined polystyrene. *Thin Solid Films* **2018**, *651*, 18−23.
(20) Ogieglo, W.; de Grooth, J.; Wormeester, H.; Wessling, M.; Nijmeijer, K.; Benes, N. E. Relaxation induced optical anisotropy during dynamic overshoot swelling of zwitterionic polymer films. *Thin solid films* **2013**, *545*, 320−326.
(21) Ogieglo, W.; Wormeester, H.; Wessling, M.; Benes, N. E. Temperature-induced transition of the diffusion mechanism of n-hexane in ultra-thin polystyrene films, resolved by in-situ Spectroscopic Ellipsometry. *Polymer* **2013**, *54*, 341−348.
(22) Murali, A.; Ganesan, M.; Satapathy, D. K.; Kumar, P. S. Penetrant-Induced Glass-like Transition in Thin Chitosan Films. *J. Phys. Chem. B* **2021**, *125*, 12617−12626.
(23) Pantelić, N.; Seliskar, C. J. Anomalous Diffusion in Poly (vinyl alcohol) - Poly (acrylic acid) Thin Films. *J. Phys. Chem. C* **2007**, *111*, 2054−2062.
(24) Lairenjam, P. D.; Sukumaran, S. K.; Satapathy, D. K. Modulation of Optical Anisotropy in Chitosan Thin Films: Role of Swelling. *Macromolecules* **2021**, *54*, 10931−10942.
(25) Bhutia, S. Z.; Lairenjam, P. D.; Sukumaran, S. K.; Satapathy, D. K. Probing the tightly bound layer in poly (vinyl alcohol) thin films using swelling measurements. *Soft Matter* **2023**, *19*, 3859−3870.
(26) Tammer, M.; Higgins, R.; Monkman, A. High optical anisotropy in thin films of polyfluorene and its affect on the outcoupling of light in typical polymer light emitting diode structures. *J. Appl. Phys.* **2002**, *91*, 4010−4013.
(27) Tammer, M.; Monkman, A. P. Measurement of the Anisotropic Refractive Indices of Spin Cast Thin Poly (2-methoxy-5-(2-ethylhexyloxy)-p-phenylenevinylene)(MEH−PPV) Films. *Adv. Mater.* **2002**, *14*, 210−212.
(28) Ramsdale, C. M.; Greenham, N. C. Ellipsometric determination of anisotropic optical constants in electroluminescent conjugated polymers. *Adv. Mater.* **2002**, *14*, 212−215.
(29) Losurdo, M.; Bruno, G.; Irene, E. A. Anisotropy of optical properties of conjugated polymer thin films by spectroscopic ellipsometry. *J. Appl. Phys.* **2003**, *94*, 4923−4929.
(30) Lin, H.-W.; Lin, C.-L.; Chang, H.-H.; Lin, Y.-T.; Wu, C.-C.; Chen, Y.-M.; Chen, R.-T.; Chien, Y.-Y.; Wong, K.-T. Anisotropic optical properties and molecular orientation in vacuum-deposited ter (9, 9-diarylfluorene) s thin films using spectroscopic ellipsometry. *J. Appl. Phys.* **2004**, *95*, 881−886.
(31) Nosal, W.; Thompson, D.; Yan, L.; Sarkar, S.; Subramanian, A.; Woollam, J. A. UV−vis−infrared optical and AFM study of spin-cast chitosan films. *Colloids Surf., B* **2005**, *43*, 131−137.
(32) Winfield, J. M.; Donley, C. L.; Kim, J.-S. Anisotropic optical constants of electroluminescent conjugated polymer thin films determined by variable-angle spectroscopic ellipsometry. *J. Appl. Phys.* **2007**, *102*, No. 063505.
(33) Ogieglo, W. *In-situ spectroscopic ellipsometry for studies of thin films and membranes*; Ph.D. thesis, University of Twente, 2014.
(34) Koziara, B. T.; Nijmeijer, K.; Benes, N. E. Optical anisotropy, molecular orientations, and internal stresses in thin sulfonated poly (ether ether ketone) films. *J. Mater. Sci.* **2015**, *50*, 3031−3040.
(35) Sosnowski, T.; Weber, H. Thin birefringent polymer films for integrated optics. *Appl. Phys. Lett.* **1972**, *21*, 310−311.
(36) Prest, W., Jr; Luca, D. The origin of the optical anisotropy of solvent cast polymeric films. *J. Appl. Phys.* **1979**, *50*, 6067−6071.
(37) Prest, W., Jr; Luca, D. The alignment of polymers during the solvent-coating process. *J. Appl. Phys.* **1980**, *51*, 5170−5174.
(38) Campoy-Quiles, M.; Etchegoin, P.; Bradley, D. On the optical anisotropy of conjugated polymer thin films. *Phys. Rev. B* **2005**, *72*, No. 045209.
(39) Woollam, J. A.; Johs, B. D.; Herzinger, C. M.; Hilfiker, J. N.; Synowicki, R. A.; Bungay, C. L. Overview of variable-angle spectroscopic ellipsometry (VASE): I. Basic theory and typical applications. *Opt. Metrol.: Crit. Rev.* **1999**, 3−28.
(40) Ogieglo, W.; Wormeester, H.; Eichhorn, K.-J.; Wessling, M.; Benes, N. E. In situ ellipsometry studies on swelling of thin polymer films: A review. *Prog. Polym. Sci.* **2015**, *42*, 42−78.
(41) Tompkins, H. G.; Hilfiker, J. N. *Spectroscopic Ellipsometry: Practical Application to Thin Film Characterization*; Momentum Press, 2015.
(42) Ata, S.; Kuboyama, K.; Ito, K.; Kobayashi, Y.; Ougizawa, T. Anisotropy and densification of polymer ultrathin films as seen by multi-angle ellipsometry and X-ray reflectometry. *Polymer* **2012**, *53*, 1028−1033.
(43) Ogieglo, W.; Wormeester, H.; Wessling, M.; Benes, N. E. Probing the Surface Swelling in Ultra-Thin Supported Polystyrene Films During Case II Diffusion of n-Hexane. *Macromol. Chem. Phys.* **2013**, *214*, 2480−2488.
(44) Huang, J.; Zajforoushan Moghaddam, S.; Thormann, E. Structural investigation of a self-cross-linked chitosan/alginate dialdehyde multilayered film with in situ QCM-D and spectroscopic ellipsometry. *ACS Omega* **2019**, *4*, 2019−2029.

https://doi.org/10.1021/acs.langmuir.4c01761
Langmuir 2024, 40, 14153−14165

(45) Tompkins, H. G.; Smith, S.; Convey, D. Optimizing the ellipsometric analysis of a transparent layer on glass. *Surf. Interface Anal.* **2000**, *29*, 845−850.
(46) Pantelić, N.; Wansapura, C. M.; Heineman, W. R.; Seliskar, C. J. Dynamic In Situ Spectroscopic Ellipsometry of the Reaction of Aqueous Iron (II) with 2, 2'-Bipyridine in a Thin Nafion Film. *J. Phys. Chem. B* **2005**, *109*, 13971−13979.
(47) Crossland, E. J.; Rahimi, K.; Reiter, G.; Steiner, U.; Ludwigs, S. Systematic Control of Nucleation Density in Poly (3-Hexylthiophene) Thin Films. *Adv. Funct. Mater.* **2011**, *21*, 518−524.
(48) Guo, S.; Gustafsson, G.; Hagel, O. J.; Arwin, H. Determination of refractive index and thickness of thick transparent films by variable-angle spectroscopic ellipsometry: application to benzocyclobutene films. *Appl. Opt.* **1996**, *35*, 1693−1699.
(49) Rahman, M. U.; Xi, Y.; Li, H.; Chen, F.; Liu, D.; Wei, J. Dynamics and structure formation of confined polymer thin films supported on solid substrates. *Polymers* **2021**, *13*, 1621.
(50) Müller-Buschbaum, P.; Stamm, M. Correlated roughness, long-range correlations, and dewetting of thin polymer films. *Macromolecules* **1998**, *31*, 3686−3692.
(51) Ogieglo, W.; Tempelman, K.; Napolitano, S.; Benes, N. E. Evidence of a Transition Layer between the Free Surface and the Bulk. *J. Phys. Chem. Lett.* **2018**, *9*, 1195−1199.
(52) Tompkins, H.; Irene, E. A. *Handbook of Ellipsometry*; William Andrew, 2005.
(53) Asada, M.; Jiang, N.; Sendogdular, L.; Sokolov, J.; Endoh, M. K.; Koga, T.; Fukuto, M.; Yang, L.; Akgun, B.; Dimitriou, M. Melt crystallization/dewetting of ultrathin PEO films via carbon dioxide annealing: the effects of polymer adsorbed layers. *Soft Matter* **2014**, *10*, 6392−6403.
(54) Sirard, S.; Green, P.; Johnston, K. Spectroscopic ellipsometry investigation of the swelling of poly (dimethylsiloxane) thin films with high pressure carbon dioxide. *J. Phys. Chem. B* **2001**, *105*, 766−772.
(55) Montiel-González, Z.; Luna-Bárcenas, G.; Mendoza-Galván, A. Thermal behaviour of chitosan and chitin thin films studied by spectroscopic ellipsometry. *Physica Status Solidi (C)* **2008**, *5*, 1434−1437.
(56) Tomkins, H. G.; McGahan, W. A. *Spectroscopic Ellipsometry and Reflectometry*; John Willey & Sons: New York, 1999; Vol. *182*.
(57) Fujiwara, H. *Spectroscopic Ellipsometry: Principles and Applications*; John Wiley & Sons, 2007.
(58) Woollam, J. A. *CompleteEASE Data Analysis Manual*; JA Woollam Co. Inc.: New England, United States of America, 2011.
(59) Jellison, G. E., Jr Data Analysis for Spectroscopic Ellipsometry. *Thin Solid Films* **1993**, *234*, 416−422.
(60) Brower, D.; Revay, R.; Huang, T. A study of X-ray reflectivity data analysis methods for thin film thickness determination. *Powder Diffraction* **1996**, *11*, 114−116.
(61) Yasaka, M. X-ray thin-film measurement techniques. *Rigaku J.* **2010**, *26*, 1−9.
(62) Mate, C. M.; Yen, B. K.; Miller, D. C.; Toney, M. F.; Scarpulla, M.; Frommer, J. E. New methodologies for measuring film thickness, coverage, and topography. *IEEE Trans. Magn.* **2000**, *36*, 110−114.
(63) Gibaud, A.; Vignaud, G.; Sinha, S. The correction of geometrical factors in the analysis of X-ray reflectivity. *Acta Crystallographica Section A: Foundations of Crystallography* **1993**, *49*, 642−648.
(64) Björck, M.; Andersson, G. GenX: An extensible X-ray reflectivity refinement program utilizing differential evolution. *J. Appl. Crystallogr.* **2007**, *40*, 1174−1178.
(65) Woollam, J. A.; Snyder, P. G.; Rost, M. C. Variable angle spectroscopic ellipsometry: a non-destructive characterization technique for ultrathin and multilayer materials. *Thin Solid Films* **1988**, *166*, 317−323.
(66) Li, Y.; Pham, J. Q.; Johnston, K. P.; Green, P. F. Contact angle of water on polystyrene thin films: Effects of CO_2 environment and film thickness. *Langmuir* **2007**, *23*, 9785−9793.

https://doi.org/10.1021/acs.langmuir.4c01761
Langmuir 2024, 40, 14153−14165